Arch. Metall. Mater. **69** (2024), 2, 425-428

DOI: https://doi.org/10.24425/amm.2024.149759

SANG-YUN SHIN[1], SEONG-HO HA[2*], DONG-HYUK KIM[2], JAEGU CHOI[2]

EFFECT OF Cu ADDITION ABOVE THE SOLUBILITY LIMIT ON MICROSTRUCTURE FORMATION AND Cu SEGREGATION IN 800 MPA GRADE DUCTILE CAST IRON DURING SOLIDIFICATION

In this study, the effect of 3 mass%Cu additions on microstructure formation and Cu segregation in 800 MPa grade ductile cast iron during solidification was investigated. The calculated phase diagram showed that after the addition of 3 mass%Cu, the Cu phase with a negligible amount appeared below 1000°C, and most Cu was included in the matrix. Based on optical microstructure, after the addition of 3 mass%Cu, the size of graphite nodules became finer, and the microstructure rarely had an area with α-ferrite. Image analysis showed that the fraction of pearlite increased significantly, indicating that Cu greatly promoted the formation of pearlite. Compositional analysis by scanning electron microscopy indicated that the pearlitic area also contained approximately 3 mass%Cu, which corresponds to those of primary and secondary austenite calculated. A small and bright phase particle containing a large amount of Cu was observed at the interface of graphite and matrix.

Keywords: 800MPa grade ductile cast iron; Graphite; Pearlite; Cementite; Copper

1. Introduction

Gray cast irons have demonstrated immense potential in various industrial applications because of their good castability, low cost, and a wide range of mechanical properties [1]. Their microstructures feature a fully pearlitic matrix with graphite particles randomly distributed in the matrix, which also provide good damping properties [1]. Different ferrite-to-pearlite ratios in the matrix can alter the properties of the alloy. A fully pearlitic matrix can be achieved by adding elements that promote metastable (pearlitic) instead of stable (ferritic) eutectoid reaction. Copper is a most used element to achieve a fully pearlitic microstructure [2-4]. Minor amounts of Cu below 1 mass% increase the volume fraction of graphite in ductile irons [5]. In addition, the content of Cu slightly above 1 mass% in ductile cast iron leads to the formation of the predominantly pearlite matrix with a high-volume fraction of graphite particles, thereby improving hardness and ultimate tensile strength [5]. Tsujikawa et al. [6] investigated the microstructure of spheroidal graphite cast iron containing copper within 0.7 mass%Cu during fertilization annealing. The influence of Sn and Cu on pearlite growth kinetics in ductile irons with a Cu content up to 0.9 mass% was studied by Lacaze and Sertucha [7]. As previously mentioned, minor concentrations of Cu for ductile cast irons have been primarily considered. However, the effect of significant amounts of Cu has been poorly examined in the last 10 years. Thus, this study focused on the microstructure formation and distribution of Cu in ductile cast irons with Cu addition above the solubility limit. This study aimed to investigate the effect of 3 mass%Cu additions on microstructure formation and Cu segregation in 800 MPa grade ductile cast iron during solidification.

2. Experimental

Iron scrap and steel scrap were charged and melted using a 125 kW high-frequency induction melting furnace and a SiC crucible. At this time, the basic composition of ductile cast iron was 3.3%C–2.1%Si–0.7%Mn–0.1%S, and Fe–Si, Fe–Mn, and Fe–S alloys were added to the molten metal during melting. In analyzing the effect of Cu addition above the solubility limit on microstructure formation during solidification, the Fe–Cu alloy was added by setting the Cu target composition of the final as-cast to 0.0 mass% and 3.0 mass%. Using an immersion thermometer attached with an R-type thermocouple, the melting temperature was kept constant between 1,480°C and 1,530°C,

[1] SBB TECH CO., LTD, GIMPO 10020, REPUBLIC OF KOREA
[2] KOREA INSTITUTE OF INDUSTRIAL TECHNOLOGY (KITECH), INCHEON 21999, REPUBLIC OF KOREA
* Corresponding author: seonghoha1999@gmail.com

and whether the temperature was raised to 1,530°C immediately before tapping was confirmed. Spheroidization was performed by adding 5.6 mass%Mg–Fe–Si alloy, and the particle-type 1.0 mass%Ba–Fe–Si alloy with a size of approximately 1.0 to 3.0 mm was used as an inoculant.

In observing the microstructure, specimens were machined in the form of a 45 mm (W) × 30 mm (D) × 5 mm (H) block by taking samples from the center of the pouring mold. The specimens were ground in the order of 100 → 300 → 600 → 1,000 → 2,000 grit using a Sic-type abrassive and finally polished in the order of 6 → 3 → 1 μm using a polycrystalline diamond and alumina-type abrasive. Thereafter, chemical etching was performed in a 3% Nital (97%C_2H_5OH–3%HNO_3) solution to analyze graphite nodularity, graphite nodule count, and matrix fraction. The graphite and matrix were observed using an optical microscope (Carl Zeiss Corporation model Axio Observer.D1m) at a magnification of 100×. In addition, microstructure observation and energy-dispersive spectroscopy (EDS)/electron backscatter diffraction (EBSD) analysis were performed using a scanning electron microscope (SEM, Carl Zeiss Corporation model Gemini 300). Moreover, phase diagram and Scheil-Gulliver cooling were calculated by *FactSage 8.2* [8].

3. Results and discussion

Fig. 1 represents phase diagrams plotted for temperature versus (a) carbon mass fraction and (b) copper mass fraction calculated by *FactSage 8.2*. At the carbon content indicated by the dashed line, the solidification begins with the formation of primary austenite, followed by the eutectic reaction of austenite and graphite. Based on the phase diagrams, cementite is often referred to as a metastable phase with regard to the graphite. However, in this study, the phase diagram is shown as calculated for the equilibrium state. After the eutectic reaction, the two-phase region with graphite and ferrite with no austenite appears at approximately 750°C, and the eutectoid reaction occurs here. According to literature [1], the eutectoid reaction occurs at 727°C: $\gamma \rightarrow \alpha + Fe_3C$. However, after the addition of 3 mass%Cu, the Cu phase appears below 1000°C. Except for the Cu phase, the existence of phases composed of other additive elements was not indicated. As shown in Fig. 1(b), the temperature of the region, including the Cu phase, increases gradually with the increase of Cu content. However, the fraction of the Cu phase remains negligibly small.

The optical microstructure of the as-cast 800-MPa-grade ductile cast irons is shown in Fig. 2. The microstructure consisted of α-ferrite and pearlite along with dispersed graphite nodules. In the absence of Cu, the α-ferrite surrounding the graphite nodules rather than pearlite dominated the microstructure, and the graphite looked well rounded. However, after the addition of 3 mass%Cu, the size of the graphite nodules became finer, and the microstructure rarely had an area with α-ferrite. Image analysis results showed that the fraction of pearlite increased significantly, indicating that Cu greatly promoted the formation

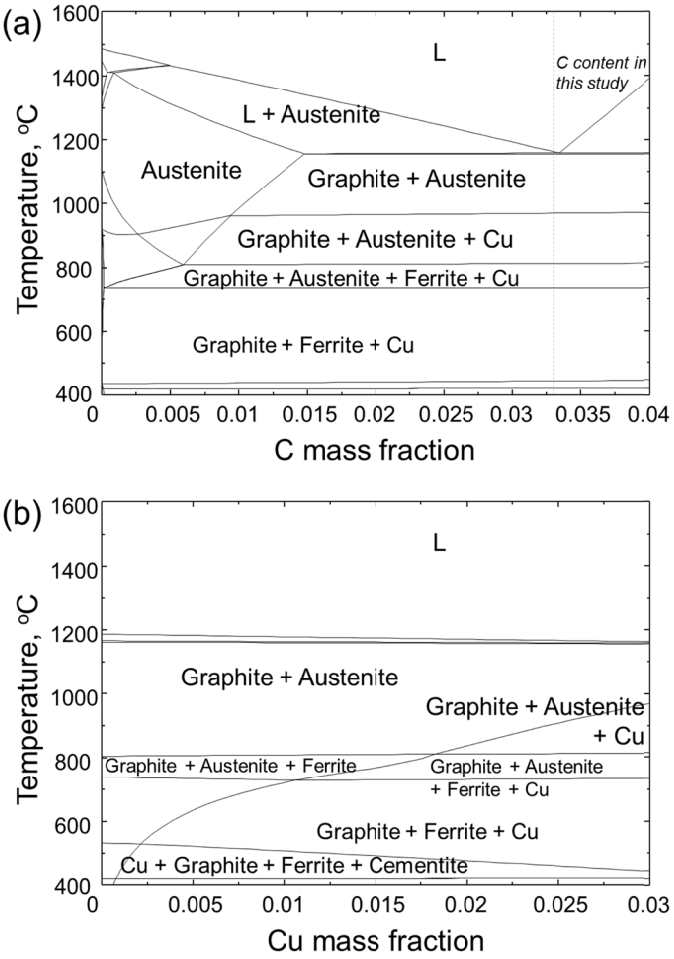

Fig. 1. Phase diagram plotted for temperature versus (a) carbon mass fraction and (b) Cu mass fraction calculated by *FactSage 8.2*. The contents of Si, Mn, and Cu are fixed at 2.1, 0.7, and 3 mass%, respectively, in Fig. 1(a). The contents of C, Si, and Mn are fixed at 3.3, 2.1, and 0.7 mass%, respectively, in Fig. 1(b)

of pearlite. In a previous study conducted by Gonzaga [9], the hardness test of cast irons indicated that hardness increased with pearlite fraction. Tsujikawa et al. [6] studied pearlite stabilization by using copper on ductile cast iron. Based on their report [6], the hardness of the ferrite phase increased with the increase of copper content by solution hardening, whereas the pearlite phase slightly increased with the increase of copper content. Therefore, the hardness will increase with the increase of pearlite phase fraction, and the addition of Cu above the solubility limit will increase the hardness of the ferrite phase in this study.

Fig. 3 shows the backscattered electron images of pearlitic areas by SEM. The composition shown in Scheil-Gulliver cooling calculated by *FactSage 8.2* and analyzed by SEM-EDS for areas indicated in Fig. 3 is shown in TABLE 1. The composition for primary austenite and secondary austenite was examined because the fractions of the two austenite phases account for almost the entire ferrous matrix. The EDS analysis result on the numbered areas shows that the detected Si content was found to be approximately 3 mass% in the pearlitic area. Compared with the cooling calculation, the measured Si content is similar to the

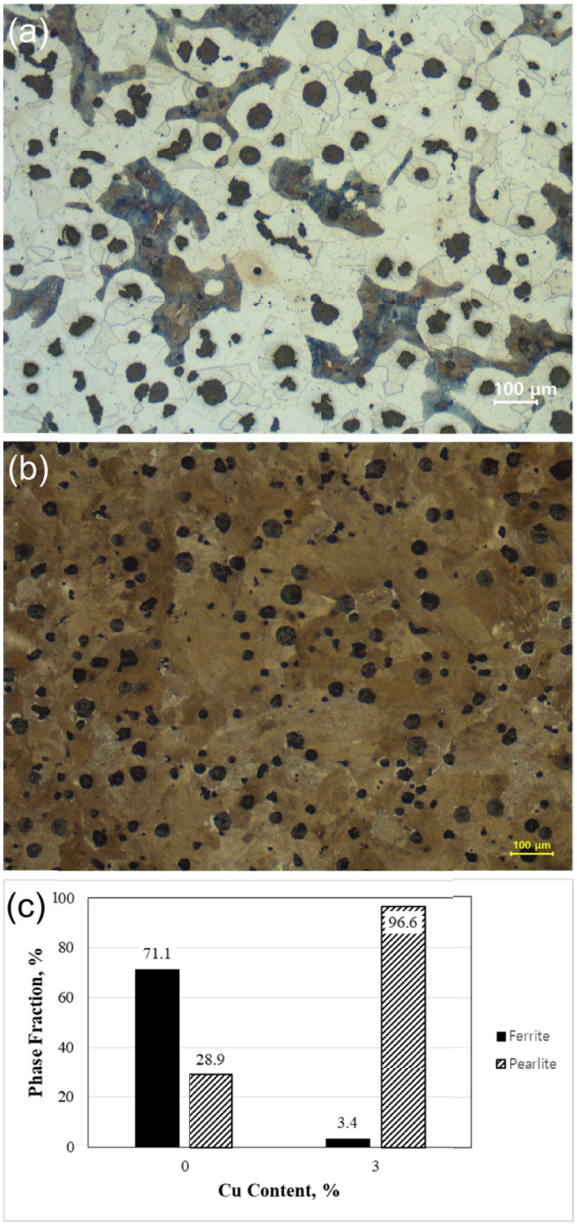

Fig. 2. Optical microstructures of as-cast 800 MPa grade ductile cast irons with (a) no Cu and (b) 3 mass%Cu. (c) Phase fraction measured by image analysis depending on Cu content

calculated one. The pearlitic area also contained approximately 3 mass%Cu, which corresponds to the calculated primary and secondary austenite. As shown in Fig. 3(b), a small and bright phase particle was observed at the interface of the graphite and matrix and found to contain a large amount of Cu. This phase is considered as the Cu phase as mentioned in the phase diagram, which was partially found only at the interface between the graphite and matrix.

TABLE 1

Composition shown in Scheil-Gulliver cooling calculated by *FactSage 8.2* and analyzed by SEM-EDS for areas indicated in Fig. 3

Phase/Area	Composition (mass%)				
	C	Si	Mn	Cu	Fe
Primary austenite*	1.46	2.37	0.53	2.43	Bal.
Secondary austenite*	1.47	2.13	0.72	3.07	Bal.
1**	—	3.47	—	3.45	Bal.
2**	32.87	0.95	—	44.55	Bal.

* Calculated, **Analyzed

Fig. 4 shows the crystallographic orientation analyzed by EBSD for the pearlitic ferrite and cementite shown in the IQ and phase maps. Spot analysis was performed at the positions for both phases indicated in the IPF map. The positions for the measurement are denoted by α for the pearlitic ferrite and θ for the pearlitic cementite (Fe_3C). The crystallographic orientation for the aforementioned positions is shown in a (001) pole figure to identify the orientation relationship between the two phases in the pearlite. According to literature [10], the quality and accuracy of the EBSD pattern for the cementite depend not only on the size and thickness of the lamellar cementite, but also on the condition of the sample surface [10]. Therefore, in this study, analysis was performed only for some areas where the EBSD pattern for the lamellar cementite was observed. The cementite analyzed in this study has a similar orientation relationship to the ferrite as in previous studies [11].

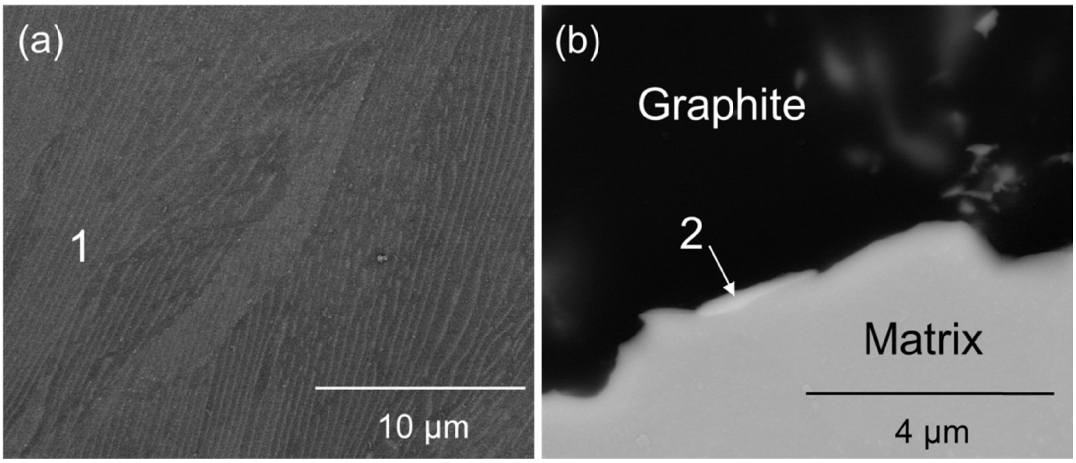

Fig. 3. SEM-backscattered electron (BSE) images of as-cast 800MPa grade ductile cast iron containing 3 mass%Cu. (a) Pearlitic area and (b) Interface between graphite and matrix

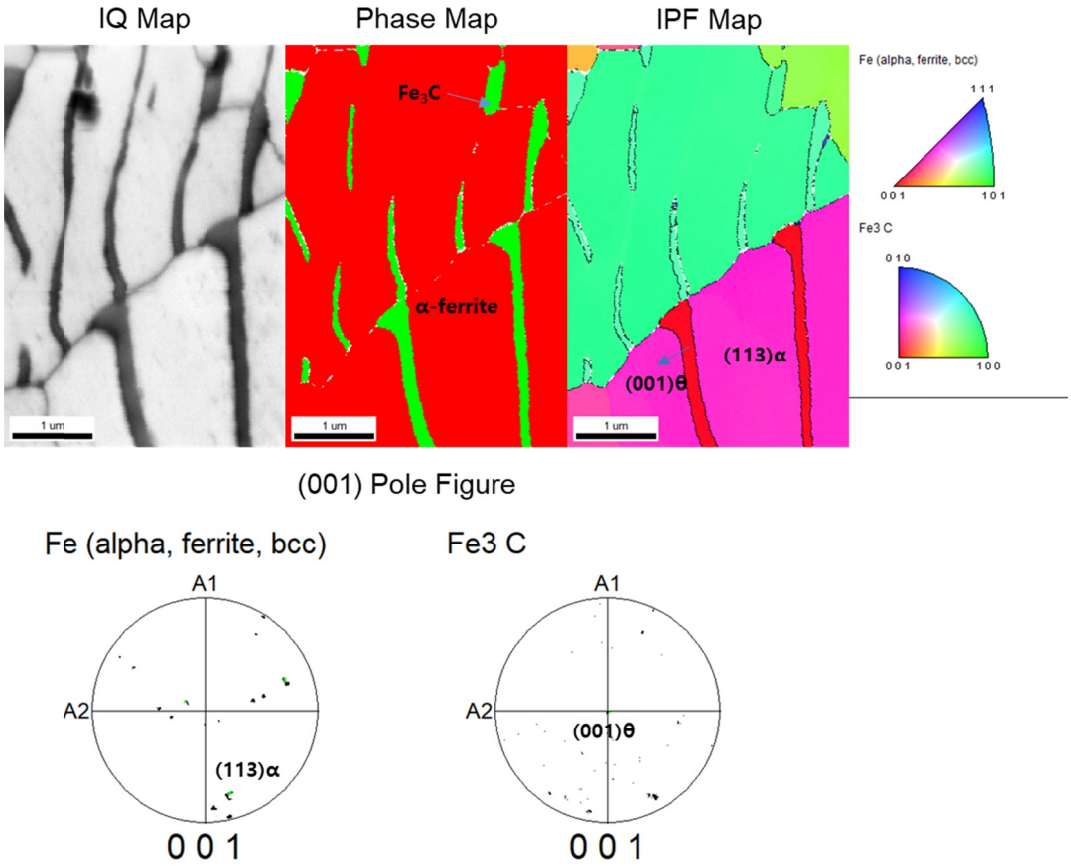

Fig. 4. EBSD images of a pearlite colony and corresponding pole figure of crystallographic orientation of ferrite (α) and cementite (θ)

4. Conclusions

The phase diagrams calculated by *FactSage 8.2* indicated that the Cu phase with a negligible amount was present below 1000°C, and most Cu was included in the matrix after the addition of 3 mass%Cu. The optical microstructures showed that the size of the graphite nodules became finer, and the microstructure rarely had an area with α-ferrite after the addition of 3 mass%Cu. The image analysis result shows that the fraction of pearlite, which is close to 100%, increased significantly and reached almost 100%, indicating that Cu greatly promoted the formation of pearlite. Compositional analysis by SEM-EDS indicated that the pearlitic area also contained approximately 3 mass%Cu, which corresponds to the calculated primary and secondary austenite. A small and bright phase particle containing a large amount of Cu was found at the interface of the graphite and matrix. In the distribution of Cu, the experimental results were consistent with the calculated results. Therefore, the addition of 3 mass%Cu above the solubility limit hardly formed a segregated phase and greatly promoted pearlite formation.

Acknowledgments

This study has been conducted with the support of the Ministry of Trade, Industry and Energy as "Materials/Parts Technology Development Program (20017503)".

REFERENCES

[1] ASM International Handbook Committee, ASM International, Properties and Selection: Irons, Steels, and High-Performance Alloys, Materials Park 1990.
[2] J.O. Agunsoye, S.A. Bello, S.B. Hassan, R.G. Adeyemo, J.M. Odii, JMMCE **2**, 470 (2014).
[3] G.I. Sil'man, V.V. Kamynin, A.A. Tarasov, Met. Sci. Heat Treat. **45**, 254 (2003).
[4] S. Abdou, A. Elkaseer, H. Kouta, J.A. Qudeiri, Adv. Mech. Eng. **10**, 1 (2018).
[5] R.K. Dasgupta, D.K. Mondal, A.K. Chakrabarti, A.C. Ganguli, J. Mater. Eng. Perform. **21**, 1728 (2012).
[6] M. Tsujikawa, N. Matsumoto, K. Nakamoto, Y. Michiura, Key Eng. Mater. **457**, 151 (2011).
[7] J. Lacaze, J. Sertucha, Int. J. Cast Met. Res. **29**, 74 (2016).
[8] C.W. Bale, E. Bélisle, P. Chartrand, S.A. Decterov, G. Eriksson, A.E. Gheribi, K. Hack, I.H. Jung, Y.B. Kang, J., Melançon, A.D. Pelton, S. Petersen, C. Robelin, J. Sangster, P. Spencer, M.A. Van Ende, Calphad **54**, 35 (2016).
[9] R.A. Gonzaga, Mater. Sci. Eng. A **567**, 1 (2013).
[10] T. Takahashi, D. Ponge, D. Raabe, Steel Res. **78**, 38 (2007).
[11] A. Durgaprasad, S. Giri, S. Lenka, S. Kundu, S. Mishra, S. Chandra, R.D. Doherty, I. Samajdar, Acta Mater. **129**, 278 (2017).